Statistical properties of separators in model active regions
by Brian Thomas Welsch

A thesis submitted in partial fulfillment of the requirements for the degree of Master of Science in Physics
Montana State University
© Copyright by Brian Thomas Welsch (1998)

Abstract:
The magnetic field in the tenuous solar corona is thought to be space-filling, since the ratio of gas pressure to magnetic pressure is much less than unity there ($/\beta = P_{gas}/P_{magnetic} \ll 1$). Observations, however, reveal enhanced X-ray/EUV emission, in the form of "transient brightenings" or "microflares," along only a small subset of field lines. Theoretical considerations suggest that these phenomena should occur along particular topological boundaries in the magnetic field, known as separators. It is along these field lines that magnetic flux is exchanged from one topological domain to another and, as a consequence of this reconnection process, energy is released as the field relaxes to a less complex state. Consequently, knowledge of a field's topological structure allows predictions about the locations and lengths of coronal X-ray/EUV loops in that field configuration.

This topological model is used to study the statistical properties of active region loops. These studies use an active region model described by the interaction of a single element of magnetic flux of one polarity with a much larger distribution of flux of the opposite polarity. The larger distribution of flux is treated in two different ways. In one, it is modelled as a continuous, mean field. In the other, it is that due to many discrete flux elements, whose randomly-chosen locations obey a Gaussian probability distribution function. In this latter case, a Monte Carlo approach was used: statistics were compiled from many realizations of such model active regions to quantify the properties of separators in a way that was insensitive to the details of any one particular distribution. The results obtained by each of these methods are compared, and simple scaling laws for separator lengths are derived. It is shown that separator lengths scale as $\sim \exp(\alpha r)/\sqrt{N}$, where N measures the flux in the large-scale distribution, and r is the distance of the single element from that distribution's center. This scaling law is a theoretical prediction of X-ray loop lengths, which can be compared with observations.

STATISTICAL PROPERTIES OF SEPARATORS
IN MODEL ACTIVE REGIONS

by

Brian Thomas Welsch

A thesis submitted in partial fulfillment
of the requirements for the degree

of

Master of Science

in

Physics

MONTANA STATE UNIVERSITY — BOZEMAN
Bozeman, Montana

April 1998

APPROVAL

of a thesis submitted by

Brian Thomas Welsch

This thesis has been read by each member of the thesis committee, and has been found to be satisfactory regarding content, English usage, format, citations, bibliographic style and consistency, and is ready for submission to the College of Graduate Studies.

Dana W. Longcope, Ph. D.   _____   4/17/98

                                                   (Signature)   Date

Approved for the Department of Physics

John C. Hermansen, Ph. D.   _____   4-17-98

                                                   (Signature)   Date

Approved for the College of Graduate Studies

Joseph J. Fedock, Ph. D.   _____   4/24/98

                                                   (Signature)   Date

STATEMENT OF PERMISSION TO USE

In presenting this thesis in partial fulfillment of the requirements for a master's degree at Montana State University-Bozeman, I agree that the Library shall make it available to borrowers under the rules of the Library.

If I have indicated my intention to copyright this thesis by including a copyright notice page, copying is allowable only for scholarly purposes, consistent with "fair use" as prescribed in the U.S. Copyright Law. Requests for permission for extended quotation from or reproduction of this thesis in whole or in parts may be granted only by the copyright holder.

Signature _Brian Welsch_

Date _4/17/98_

TABLE OF CONTENTS

LIST OF FIGURES

ABSTRACT

The magnetic field in the tenuous solar corona is thought to be space-filling, since the ratio of gas pressure to magnetic pressure is much less than unity there ($\beta \equiv P_{gas}/P_{magnetic} \ll 1$). Observations, however, reveal enhanced X-ray/EUV emission, in the form of "transient brightenings" or "microflares," along only a small subset of field lines. Theoretical considerations suggest that these phenomena should occur along particular topological boundaries in the magnetic field, known as separators. It is along these field lines that magnetic flux is exchanged from one topological domain to another and, as a consequence of this reconnection process, energy is released as the field relaxes to a less complex state. Consequently, knowledge of a field's topological structure allows predictions about the locations and lengths of coronal X-ray/EUV loops in that field configuration.

This topological model is used to study the statistical properties of active region loops. These studies use an active region model described by the interaction of a single element of magnetic flux of one polarity with a much larger distribution of flux of the opposite polarity. The larger distribution of flux is treated in two different ways. In one, it is modelled as a continuous, mean field. In the other, it is that due to many discrete flux elements, whose randomly-chosen locations obey a Gaussian probability distribution function. In this latter case, a Monte Carlo approach was used: statistics were compiled from many realizations of such model active regions to quantify the properties of separators in a way that was insensitive to the details of any one particular distribution. The results obtained by each of these methods are compared, and simple scaling laws for separator lengths are derived. It is shown that separator lengths scale as $\sim \exp(\alpha r)/\sqrt{N}$, where N measures the flux in the large-scale distribution, and r is the distance of the single element from that distribution's center. This scaling law is a theoretical prediction of X-ray loop lengths, which can be compared with observations.

CHAPTER 1

INTRODUCTION

HOW IS THE CORONA HEATED?

Physicists still do not understand how the solar corona is heated to a temperature of several million kelvins (MK), while the chromosphere, immediately beneath it, is two orders of magnitude cooler. One of two mechanisms is generally held to be responsible. In one view, magnetoacoustic or Alfvén waves (Osterbrock 1961), carry energy from the convection zone, through the chromosphere, and deposit it in the corona. Heating models employing waves, however, face serious difficulties, most notably the "disinclination" of Alfvén waves to deposit energy in the corona (Parker 1988 ; Porter, Klimchuk, & Sturrock, 1994).

In the other view of coronal heating, energy is dissipated directly in the corona as a by-product of some process involving the reconnection of magnetic field lines. At present, however, no known mechanism would allow reconnection to occur in the highly conductive corona. Nonetheless, detailed observations in X-ray (Lin et al. 1984), $H\alpha$ (Canfield & Metcalf 1987), and simultaneous observations in X-ray and UV (Porter & Klimchuk 1995) have shown that aperiodic events on small spatial scales and short time scales, consistent with reconnection processes, regularly deposit $\sim 10^{27}$ ergs of energy in the corona, suggesting that small-scale, flare-like events might be heating the corona. Since this energy is $\sim 10^{-6}$ that typically seen flares, the term "microflares" has been associated with these phenomema.

Short-term heating of X-ray loops, in the form of "transient brightenings," are also regularly seen in images taken with the soft X-ray telescope (SXT) on board the Yohkoh satellite (Shimizu et al. 1992). These events typically last for a few minutes, and occur with frequencies ranging from one every few minutes to one per hour, depending on just how "active" the host active region is (Shimizu et al. 1992).

Such events are typified by an initial brightening of loop footpoints that leads to brightening of the entire loop, and simultaneous brightenings in multiple loops are not uncommon. For these reasons, Shimizu (1994) attributes these phenomena to "the magnetic interaction of multiple loops."

The fact that estimates of the energy released in these events, $10^{25} - 10^{29}$ ergs (Shimizu 1995), are near estimates of the energy released in microflares (Porter & Klimchuk 1995) has led some (Gary, Hartl, & Shimizu 1997) to speculate that these two flare-like phenomena are, in fact, identical.

Nomenclature aside, these events contribute significantly to coronal heating above active regions. While Porter (1995) argues only that microflares "cannot be dismissed" as a component of active region heating processes, Shimizu (1995) has placed an upper bound on the total energetic contribution of transient brightenings to active region heating at about 20 % of that required to account fully for active region temperatures.

One puzzling aspect of these phenomena is that the mechanism responsible for the brightenings is quite selective. Because the gas pressure in the tenuous corona is much less than the pressure due to the magnetic field there ($P_{gas}/P_{magnetic} \equiv \beta \ll 1$), the magnetic field is believed to fill the entire coronal volume. But the coronal plasma is bright in X-rays along only a few of the field lines above an ordinary active region, as may be seen in the example shown in Figure 1.

Magnetic Charge Topology

Where does the energy that is released in these transient brightenings and microflares originate? The structure of the coronal magnetic field is primarily a product of the distribution of the field at the photosphere. Flux elements seen in magnetograms are interpreted as the cross sections of slender flux tubes whose tops have emerged into the corona (Parker 1955; D'Silva & Choudhuri 1993; Fan, Fisher & McClymont 1994; Caligari, Moreno-Insertis, & Schüssler 1995). Models suggest (Gabriel 1976) that, in the low β plasma above the photosphere, the isolated flux tubes expand to fill space. In the accepted view of flare energetics, photospheric plasma flows
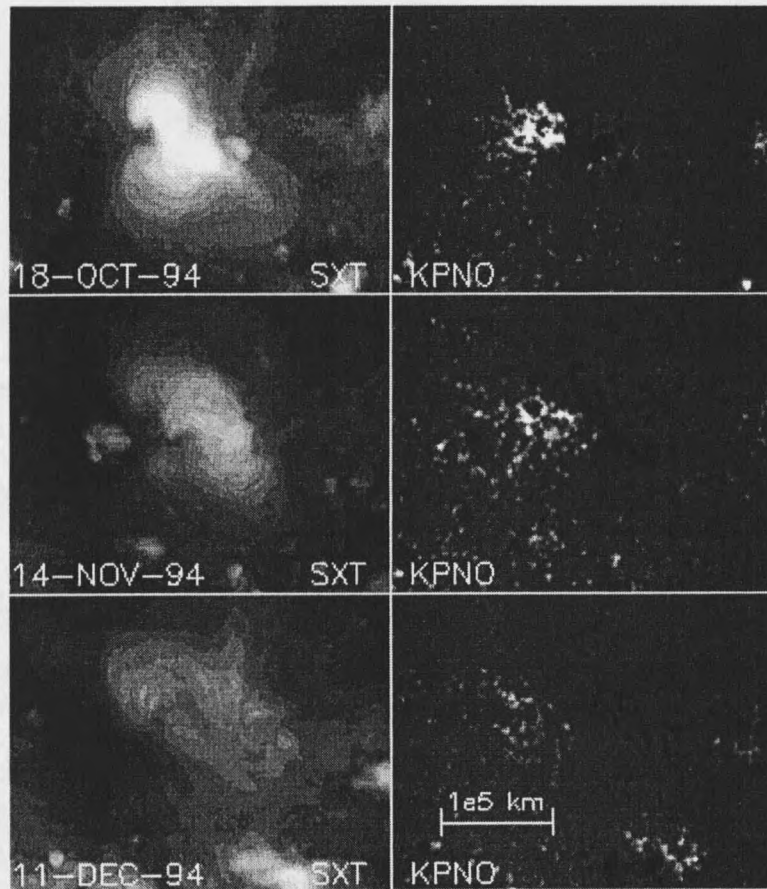
Figure 1: Yohkoh SXT images of an active region, juxtaposed with Kitt Peak line-of-sight magnetograms of the same active region, over three successive solar rotations. (This active region was assigned NOAA AR # 7790 on its first pass). Because the gas pressure is so slight in the tenuous corona ($P_{gas}/P_{magnetic} \equiv \beta \ll 1$), magnetic fields above the active region fill all space. Obviously, however, only a few field lines are bright in soft X-rays. Why? (Courtesy Loren Acton.)

shuffle the locations of these magnetic flux elements. This increases the complexity of the coronal field, gradually increasing the stress, and, hence, the energy stored in that field (Gold & Hoyle 1960; VanHoven et al. 1980). When this energy is suddenly released into the corona, we observe its signature in various ways, most notably in enhanced coronal emission.

The energy release in microflares, like that in "true" flares, is impulsive (Porter & Klimchuk 1995). Further, in both cases, particles are accelerated with sufficient energy to generate X-rays characteristic of $T \sim 10$ MK plasmas. These qualitative similarities suggest that microflares are indeed members of the "flare family" (Porter & Klimchuk 1995). We therefore assume that energy released in microflares and transient brightenings was stored in field stresses before these events.

Since the build-up of stress in the field is typically a rather slow process, the long time scales and small electric fields involved mean the approximations of ideal magnetohydrodynamics (MHD) apply (Longcope 1996). Due to the complexity of coronal fields, theoretical models must include further idealizations to simplify the process of energy storage and release. One approach is to consider simple footpoint distributions (e.g., Hood & Priest 1979) or those exhibiting a high degree of symmetry (e.g., Low 1977).

Another approach, adopted here, involves two assumptions. The first assumption is that the coronal magnetic field is current-free,

$$\mathbf{J} = \nabla \times \mathbf{B} = 0 \ , \tag{1}$$

meaning it may be represented by the gradient of a scalar potential field,

$$\mathbf{B} = -\nabla \chi \ . \tag{2}$$

In the second assumption, we take the coronal field to be that which would arise if the flux elements at the photosphere were point-like "magnetic charges,"

$$\mathbf{B} = \sum_{i=0}^{N} \frac{q_i (\mathbf{x} - \mathbf{x'}_i)}{|\mathbf{x} - \mathbf{x'}_i|^3} \ , \tag{3}$$

where $\Psi_i = 2\pi q_i$ is the flux in footpoint i, and $\mathbf{x'_i}$ is its location. The field in the corona is then uniquely determined by the solution of Laplace's equation,

$$\nabla \cdot \mathbf{B} = -\nabla^2 \chi = 0 \ , \tag{4}$$

where the distribution of discrete flux elements at the photosphere is imposed as a boundary condition.

By grouping field lines according to their endpoints, classes of field lines are delineated by the various linkages that are possible. In this framework, Sweet (1958) showed that well-defined boundaries exist between basins of differing connectivity, and termed these boundaries *separatrices* and *separators*. Baum & Bratenahl (1980) first quantified the description of the field in topological terms; several authors have since revisited and refined their approach (Gorbachev & Somov 1988; Priest & Forbes 1989; Somov 1992; Lau 1993; Demoulin, Hénoux, & Mandrini 1994; Parnell, Priest, & Golub 1994). Descriptions of magnetic fields in these terms have been grouped under the rubric of *magnetic charge topology* (MCT, Longcope 1996).

These topological boundaries are expected to be the loci of the greatest stresses in the coronal field as photospheric motions rearrange the field's footpoints. Hence, they are the most likely sites of reconnection and consequent energy release, seen in the form of flares and microflares (Longcope 1996). In this context, the selective brightening mechanism revealed in the images in Figure 1 makes sense: field lines near separators emit more energy in the form of X-rays than other field lines because more energy is being deposited there than elsewhere.

In this work, we employ the techniques MCT to make semi-empirical predictions of statistical properties of separators as they would occur in solar active regions. This is the first step in a larger calculation, that of coronal heating rates due to reconnection along separators in active regions. In this work, we calculate the expected length distribution of separator loops occuring in simple models of active regions. These statistical properties can be ascribed to observed coronal X-ray loops. We explore their dependence on quantities one can assign to every active region: size, flux, and number of constituent flux elements.

Shimizu (1994) has compiled statistics on the lengths of coronal loops observed with SXT. As the first step toward an explanation of his results on the basis of theory alone, this investigation is the first theoretical study of its kind. It is also a test of the validity of the MCT model. The work presented here forms the basis of further investigations, already underway, involving more complex models of active regions.

In the next chapter, we describe the separator model in much more qualitative detail, first defining the topological entities to which the model refers, and then briefly discussing energetics in this model. In Chapter 3, we find separator lengths in active regions in which the large-scale fields are approximated by mean fields. In Chapter 4, we find separator lengths in model active regions composed of many flux elements, without averaging. Finally, in the last chapter, we compare and discuss the results obtained with the two different methods.

CHAPTER 2

THE SEPARATOR MODEL

A SINGLE CHARGE IN A BACKGROUND FIELD

To introduce topological field models, we first consider a single magnetic "test" charge q_B, located at the photospheric surface. We suppose the charge is immersed in a uniform, horizontal background field, which points in what we define to be the $\hat{\mathbf{x}}$ direction, $\mathbf{B} = B_0\hat{\mathbf{x}}$. For concreteness, we suppose the polarity of the test charge is negative, and, further, that it is located at the origin.
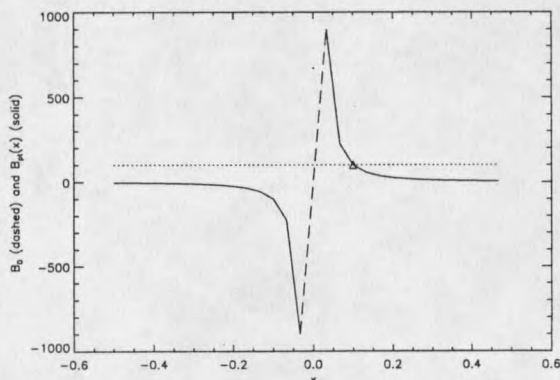
Figure 2: Plots of the constituents of B_x along the $\hat{\mathbf{x}}$ axis: the dotted line is the background field $B_x = B_0$, here given the arbitrary value of 100, while the solid line is $B_x = -(B_{\text{pt}}(x, 0, 0))_x = -q_B/x^2 = +1/x^2$. (The dashed line connects the field of the latter across the field singularity at the charge.) The two curves must intersect at one point; at that point, denoted x_*, the fields cancel, meaning x_* is a *null* point, shown here as a ($\triangle$).

Both the B_y and B_z components of the field vanish identically along the $\hat{\mathbf{x}}$ axis. The remaining component, B_x, vanishes at the point $\mathbf{x}_*$, at which

$$B_0 = \frac{q_B}{|\mathbf{x}_*|^2} = \frac{q_B}{x_*^2} \; , \tag{5}$$

with $\mathbf{x}_* = (x_*, 0, 0)^T$, where $x_* > 0$ (see figure (2)). The location of the null is then easily seen to occur at

$$x_* = \sqrt{\frac{q_B}{B_0}} \ . \tag{6}$$

Most field lines in this configuration can be grouped into two categories, according to their endpoints: 1) field lines which start at negative infinity and end at q_B, i.e., those field lines which connect the background field to q_B; and 2) field lines constituting the background field, i.e., those with both endpoints far from the test charge. Field lines which constitute the boundary between these two domains can end
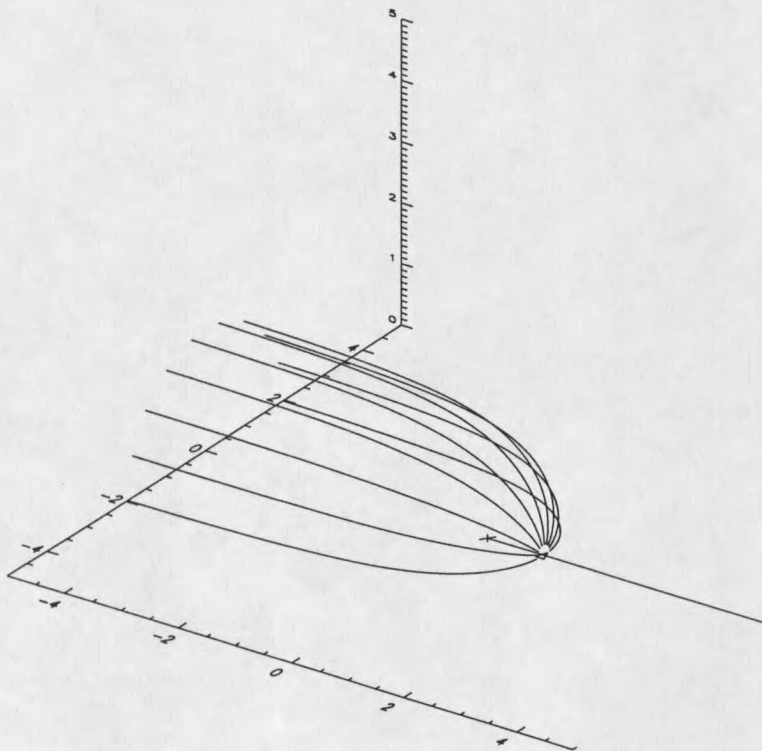
Figure 3: A selection of field lines on test charge's separartrix surface: they begin at $-\infty$, and end at the null at $\mathbf{x}_*(\triangle)$. Collectively, we label all the lines in the surface Σ. All field lines within the separatrix begin at $-\infty$ and end at the test charge, while all those without begin at $-\infty$ and end at $+\infty$. Also shown are the null's γ-lines, the field lines that leave the null: one runs from the null to the test charge, while the other runs to $+\infty$.

at neither q_B nor infinity, and thus fall into a third category: they begin at negative

infinity and end at the location of the null, $\mathbf{x}_*$. These field lines form the test charge's *separatrix surface*, which we label Σ (Figure 3).

PROPERTIES OF NULL POINTS

Near the null, the magnetic field can be expanded in a Taylor series,

$$\mathbf{B}(\mathbf{x}_* + \Delta\mathbf{x}) = \mathbf{M}(\mathbf{x}_*) \cdot \Delta\mathbf{x} + \cdots \quad , \tag{7}$$

where the elements of the Jacobian matrix $\mathbf{M}(\mathbf{x}_*)$ are $M_{ij} = \frac{\partial B_i}{\partial x_j}|_{x_*}$. Since the field is force-free, the matrix is symmetric and thus has three real eigenvalues, and three orthogonal eigenvectors (Longcope 1996). As $\nabla \cdot \mathbf{B} \equiv 0$, two eigenvalues must differ in sign (Cowley 1973; Yeh 1976), and the sign of the third delineates two classes of nulls (Cowley 1973): a null is A-type if two eigenvalues are negative, and B-type if two are positive.

This delineation of two classes of nulls, based upon the sign of the intermediate eigenvalue of the Jacobian matrix, neglects the possibility that this eigenvalue may vanish. The null in such a case is not *generic*; we digress to discuss briefly this eventuality. Consider a null in some configuration in which the intermediate eigenvalue of the Jacobian though small, is nonzero. By changing the amplitude of a charge near the null, both the null's location and the Jacobian are perturbed. When the intermediate eigenvalue is sufficiently small, such a perturbation can change the sign of the eigenvalue. If so, the null undergoes a pitchfork bifurcation: two nulls of the same type as the original appear, one just above and one just below the photosphere, and another of the opposite type appears in place of the old. These bifurcations are in fact seen in numerical simulations; as the properties of such configurations are beyond the scope of the current theory, however, only generic cases are considered in all that follows.

In general, field lines leave (enter) an A-type (B-type) null along two lines which run in opposite directions along the eigenvector corresponding to the null's sole positive (negative) eigenvalue. These are the null's γ-lines, or "spines" (Parnell, Priest, & Golub 1994) one runs from (to) the null to (from) the charge, while the other is

connected to a charge that gives rise to part of the background field. Clearly, then, an A-type (B-type) null is associated with a negative (positive) charge. Since the null at x_* is A-type, we rename its location x_A.

At a microscopic level, very near the null, field lines enter (leave) an A-type (B-type) null in the two-dimensional surface spanned by the two negative (positive) eigenvectors, forming a so-called "fan" (Parnell, Priest, & Golub 1994) in a plane. Further from the null, the macroscopic field deforms the flat plane into a curved surface.

Field lines on a given side of this surface have an endpoint at the same charge that the γ-line on that side of the surface does. This means that the separatrix forms the boundary between field lines having different connectivity. Hence, a given charge's separatrix demarcates the volume which contains all of that charge's flux.

In our example, the eigenvectors corresponding to the negative eigenvalues of M at A are perpendicular to the $\hat{x}$-axis, and the separatrix surface is thus locally tangent to a plane parallel to the $y - z$ plane. This tangent plane bisects the $\hat{x}$-axis at x_A.

What we have been calling "the background field" must, ultimately, be due to another charge or charges. Hence, we have in fact been considering a configuration of at least two charges. How did we associate "the null" with "the charge"? We digress to consider this question. In a configuration with multiple charges, and only generic nulls, one can argue that the number of nulls is one fewer than the number of charges. The presence of an "orphan" charge notwithstanding, however, it is in principle possible to associate a particular null with each charge, and vice versa. To understand this, imagine that a charge is added to a configuration of charges by being "turned on," in the sense that its amplitude is raised from zero in small steps. The instant the charge appears, a null also appears, quite near the charge, and the two are easily associated merely by their proximity: their separation is given by equation (6). (One can imagine, however, that, as the charge's amplitude is increased further and the null-charge separation increases, the null can move away from the charge in a way that is not easy to predict, due to variations in the background field. Consequently, in practice, it is nontrivial to find the null associated with a particular charge in a

given configuration.)

Intersection of Separatrix with Photosphere

Much of the work presented on the following pages involves the field lines at the intersection of a test charge's separatrix with the photosphere. It is therefore appropriate to derive the equation of this curve, which we label $\mathcal{C}_\Sigma$, in the monopole example now, for comparison to work discussed below. The easiest way to proceed takes advantage of the symmetry of this configuration to represent the fields using Clebsch variables (Moffatt 1978). It is expedient to operate in a cylindrical coordinate system, $(\rho'(x, y, z), \phi'(x, y, z), z'(x, y, z))$, where the following transformations give the new coordinates in terms of the old:

$$\rho' = \sqrt{y^2 + z^2} \tag{8}$$

$$\phi' = tan^{-1}\left(\frac{y}{z}\right) \tag{9}$$

$$z' = x \tag{10}$$

In the new coordinates, the field is symmetric about the $\hat{z}'$-axis, and can be written in terms of a flux function, $f(\rho', z')$:

$$\mathbf{B}(\rho', \phi', z') = \nabla f \times \nabla \phi' = -\frac{1}{\rho'}\hat{\phi}' \times \nabla f \ , \tag{11}$$

where the gradient is in cylindrical coordinates. The flux function is the sum of contributions from the uniform background field and the point charge,

$$f^{(\mathrm{b})} = -\frac{(\rho')^2}{2}B_0 + f_0^{(\mathrm{b})} \tag{12}$$

$$f^{(\mathrm{pt})} = -\frac{q_B z}{\sqrt{(\rho')^2 + (z')^2}} + f_0^{(\mathrm{pt})} \tag{13}$$

$$\Longrightarrow f = -\frac{(\rho')^2}{2}B_0 - \frac{q_B z}{\sqrt{(\rho')^2 + (z')^2}} + f_0^{(\mathrm{b})} + f_0^{(\mathrm{pt})} \ . \tag{14}$$

In what follows, we take the (arbitrary) constants that appear in the equation above, $f_0^{(\mathrm{b})}$ and $f_0^{(\mathrm{pt})}$, to be zero. The advantage of this formulation is that contours of f are field lines. So, to find the equation of the field lines that form $\mathcal{C}_\Sigma$, we evaluate f at

the coordinates of A in the new system, $(0, \sqrt{q_B/B})$,

$$f\Big|_A = f\left(0, \sqrt{\frac{q_B}{B_0}}\right) = -q_B \quad , \tag{15}$$

and then solve for $\rho'(z')$, since

$$\frac{q_B z'}{\sqrt{(\rho')^2 + (z')^2}} + \frac{B_0}{2}(\rho')^2 = q_B \tag{16}$$

obtains along this field line. Defining $a \equiv \sqrt{\frac{q_B}{B_0}}$, this can be written

$$\left(1 - \frac{(\rho')^2}{2a^2}\right)^2 = \frac{(z')^2}{\rho^2 + (z')^2} \quad , \tag{17}$$

which, after a little algebra, reduces to

$$(\rho')^2\left[1 - \frac{(\rho')^2}{2a^2}\right]^2 = (\rho')^2\frac{(z'^2)}{a^2}\left[1 - \frac{(\rho')^2}{4}\right] \quad . \tag{18}$$

Because both the null's γ-lines and $\mathcal{C}_\Sigma$ run through the null, f takes the same value on both. Since we want the equation for $\mathcal{C}_\Sigma$, we must factor out the solutions for the γ-lines, which run along the axis ($\rho' = 0$). Doing so leaves a bi-quadratic in $\rho'(z')$,

$$1 - \frac{(\rho')^2}{a^2} + \frac{1}{4}\frac{(\rho'^4)}{a^4} = \frac{(z')^2}{a^2} - \frac{1}{4}\frac{(\rho')^2}{a^2}\frac{(z')^2}{a^2} \quad ,$$

which yields, after application of the quadratic equation,

$$\frac{(\rho')^2}{a^2} = 2\left[\left(1 - \frac{1}{4}\frac{(z')^2}{a^2}\right) \pm \sqrt{\frac{1}{2}\frac{(z')^2}{a^2} + \frac{1}{16}\frac{z'^4}{a^4}}\right] \quad . \tag{19}$$

In Figure 4, we have plotted $\rho'(z')$, which is a cross section of the test charge's separatrix surface.

The $(-)$ root gives the correct $\rho'(z')$ for z' on $[0, a]$, while the $(+)$ root yields $\rho'(z')$ on $z = (-\infty, 0)$. When $z' \ll 0$, and $|z'| \gg a$, one can factor $(\frac{z'}{2a})^4$ out of the radical and expand the result in a binomial series, which gives, to order $(\frac{a}{z'})^2$:

$$\frac{(\rho')^2}{a^2} = 2 - \frac{(z')^2}{2a^2} + \frac{(z')^2}{2a^2}\sqrt{1 + \frac{8a^2}{(z')^2}} \tag{20}$$

$$\simeq 2 - \frac{(z')^2}{2a^2} - \frac{(z')^2}{2a^2} + \frac{(z')^2}{2a^2}\left(\frac{4a^2}{(z')^2}\right) = 4 \tag{21}$$

$$\implies \rho'(\infty) = 2a \tag{22}$$